Attitude recovery from feature tracking for estimating angular rate of non-cooperative spacecraft

Attitude recovery from feature tracking for estimating angular rate of non-cooperative spacecraft

G. Biondi, S. Mauro, T. Mohtar, S. Pastorelli, M. Sorli

Politecnico di Torino[a], Dipartimento di Ingegneria Meccanica e Aerospaziale[a]

[a]10129 Corso Duca degli Abruzzi 24, Torino

Abstract

This paper presents a fault-tolerant method for estimating the angular rate of uncontrolled bodies in space, such as failed spacecrafts. The bodies are assumed to be free of any sensors; however, a planned mission is assumed to track several features of the object by means of stereo-vision sensors. Tracking bodies in the space environment using these sensors is not, in general, an easy task: obtainable information regarding the attitude of the body is often corrupted or partial. The developed method exploits this partial information to completely recover the attitude of the body using a basis pursuit approach. An unscented Kalman filter can then be used to estimate the angular rate of the body.

Keywords: Space debris, Stereo-vision, Basis pursuit denoising, State estimation, Signal recovery

1. Introduction

The estimation of attitude and angular rate of artificial satellites is a very well-known process that is normally performed using the appropriate on-board instrumentation. Very common associated techniques are sensor fusion and Kalman filtering; data captured by star trackers and gyros are combined with dynamic models of the system to produce an on-orbit estimate of the state,

URL: www.polito.it (Politecnico di Torino)

which includes the inertia tensor, which changes over time because of fuel consumption [1]. This information is required for stability control of the active spacecraft. Several studies have been peformed to relieve some of the used sensors to prevent failures and to reduce costs, particularly for missions involving small spacecrafts [2]. Additionally, gyro-less control systems that use only star tracker information as the input of accurate non-linear Kalman filters have been developed.

The estimation problem becomes difficult when artificial objects have no active sensors at all,*i.e.*, in the case of failed spacecrafts. No direct information regarding the attitude of the object might be available and obtaining this information by exploiting external sensors (*e.g.*, CCD cameras on a chaser spacecraft) is, in general, a difficult task.

Space debris removal is becoming an urgent environmental issue related to space exploration. As assessed by the U.S. Space Surveillance System, the number of objects that orbit the Earth has increased significantly over the years [3]; the risks of collisions between active and lost spacecrafts may soon become consistent. Additionally, no docking or de-orbiting maneuver can be considered safe without precise knowledge of the attitude and angular rate of the target debris. Lichter and Dubowsky [4] proposed an architecture for the estimation of the dynamic state of non-cooperative spacecrafts. This architecture primarily consists of 3D active sensors, which are suitable for use in harsh lighting conditions. Aghili *et al.* [5] presented a method for pose estimation of passive space bodies using a laser 3D scanner. Their method also considers the possibility of failures during the scanning procedure without compromising the estimation. However, this method requires a CAD model of the object.

The use of active sensors, although they are relatively reliable, could nevertheless be less appealing than obtaining the same information using stereo-vision sensors, because of the possibility of saving energy and costs. A survey of the most common tracking techniques based with stereo-vision can be found in [6]. In [7] and [8] two different methods are presented to maintain a target space body in the field of view (FOV) of cameras on a chaser spacecraft after the

rendezvous phase. In these studies, estimation of the angular rate is not performed. Both of the methods seem to be applicable over a relatively long time period. The main drawback of methods that exploit stereo-vision cameras is that different phenomena (such as occlusions or disturbing reflections) cause discontinuous tracking of the natural features of space objects. In spite of this, recently, several authors have attempted to prove the effectiveness of these systems.

In [9] a 3D-model-matching technique, as used in [5], is combined with stereo-vision sensors. The considered method requires a large number of detected features and a very detailed model of the failed satellite. In [10], a powerful method based on stereo vision to track a non-cooperative spacecraft and to estimate its complete dynamic state is presented. The method does not require any *a-priori* information about the target; however, it is assumed that the positions of several features are always measurable. For that reason, although the method has shown very good accuracy, it would be not applicable if occlusions occur during tracking or if in some instant of time the detectable features are less than three.

In [11], the tracking of a target body relative to a chaser is achieved via the prediction of the velocities of its features. This prediction is based on a kinematic model of the object. In this work, the problem of recovering the pose and the angular rate of the object during occlusions is considered; however, no results are shown in the case in which no features are detectable. Moreover, when the number of detected features decreases, the precision of the estimation significantly decreases. The paper states, however, that the prediction is useful for re-initializing the tracking.

The work presented in [12] considers the determination of the relative pose between a chaser and a larger target that are cooperative. This work is interesting for two reasons: tracking is performed using stereo-vision cameras and when occlusions occur, although the attitude information is lost, the position of the body is predicted using a mathematical model of the body itself. The tracking can then continue after the occlusion periods; however, the pose of the object

is not obtained in these periods. An important assumption underlying the cooperativeness between the spacecrafts is that the positions of certain artificial features on the target (in the case considered, LEDs) are known *a-priori*.

Definitely, the current state of the art appears to be missing of fault-tolerant methods for attitude estimation from features detected by means of stereo cameras. The method proposed in this paper offers the possibility of recovering attitude information of a space body such as a failed spacecraft; the continuity of the feature tracking is not required, so the method is applicable to recover the object pose also if momentary failures in feature detection occur. The method can also be applied in conditions similar to those in [12].

The fundamental assumption that allows the presented algorithm to succeed is the ability to track several features (*i.e.*, corners, edges, tips, or other recognizable parts) of the object using two cameras on a controlled chaser spacecraft. Measurements must be available at least for frequent and short intervals of time. Data samples should consist, in particular, of the Euclidean coordinates of the features with respect to a reference frame with the origin in the center of mass of the chaser. This hypothesis seems to be reasonable considering the previously mentioned state of the art.

Another assumption concerns knowledge of the relative positions between the detected features. This knowledge can be achieved during tracking: if a 3D model of the object is available, it is possible to associate the few detected features with the corresponding points on the model. It is not necessary that the model be highly detailed, as only a small number of features need be recognized. For example, in [13], sequential photographs of a passive space body provide knowledge of the pose of the camera with respect to a 3D model of the object. This method allows recognition of the correspondences between detected features and specific points on the model. If no model is available, the relative positions could be estimated by averaging many measurements and by constraining the distances between detected features to be constant. This last method is difficult to achieve because it would require that the tracking architecture be capable of associating each feature with a unique label and recognizing

it when it is detected.

The principle underlying the procedure is as follows: once a corrupted attitude signal is generated from the input data, it is possible to recover the signal by converting this operation into a non-linear optimization problem under the assumption that the original signal can be treated as the composition of a small number of elementary signals. This approach is common in signal processing, especially in fields such as image recovery, signal decoding, and signal deconvolution. This approach has also been successfully used for solving prognostic problems related to mechanical systems such as gear boxes [14], [15]. However, this technique has seldom been applied to the estimation of kinematic quantities from raw data. Additionally, it uses one of the most effective existing approaches [16], *i.e.*, the basis pursuit approach. This method is quite adaptable to situations in which signals are affected by noise (*basis pursuit denoising*); it has been proven, through numerical simulations, to be very effective in the recovery of attitude signals. The optimization problem is solved using a fast and reliable algorithm, SALSA [17], an acronym of split augmented Lagrangian shrinkage algorithm.

Once the attitude is available, the angular rate can then be estimated via classical methods based on Kalman filtering, because of the strict correlation between angular rate and attitude. However, this last aspect is not the main purpose of the paper; the main intent consists instead in proposing a novel method for recovering the attitude from features also in the case of temporary losses of measured data.

The remainder of this paper is organized as follows. In the second section, we provide a general overview of the problem solved in this paper. Additionally, we describe how a realistic input data set could be created when field measurements are not available; simulated data are also used to calculate an expected output so as to validate the algorithm results. In the third section, the theoretical fundamentals of basis pursuit denoising are presented together with a brief description of the algorithm used to solve the basis pursuit problem. In the fourth section, we describe how all of the proposed theories are applied for

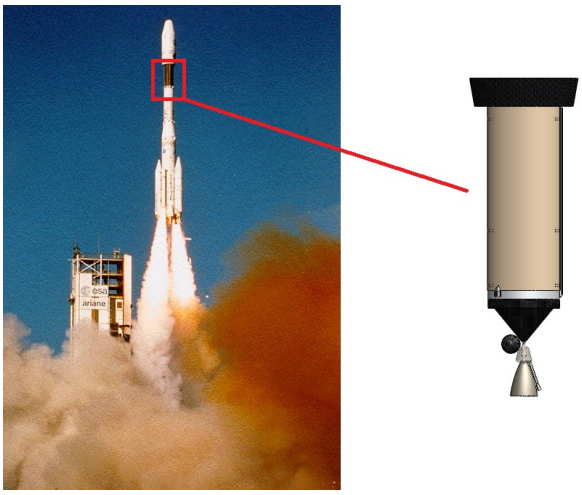

Figure 1: Third stage of Ariane 4, H10.

the estimation of the attitude of a generic body. Additionally, in section five, we describe an unscented Kalman filter for estimating the angular rate, and provide an example of the results of the procedure. Finally, section six presents our conclusions.

2. Problem statement and tracking simulation

The approach used to achieve our objectives uses identification algorithms with simulated data as inputs. These data are created by applying mathematical models. In particular, two models have been created: a model for the target and a model for the chaser. The model of the target is used to identify plausible trajectories of some of its characteristic points. The realistic perspective target chosen is the third stage, H10, of the expendable launch system Ariane 4 [18] (see figure 1). This object is $11.53m$ high, $2.66m$ in diameter, and $12000kg$ in gross mass. Combining this model with that of the chaser, it is possible to identify the relative orientation and position of the objects. It is also possible to determine which points are visible from the chaser. The addition of noise to these trajectories provides a set of realistic data that serve as input to the identification algorithms. Figure 2 presents the procedure described above. The

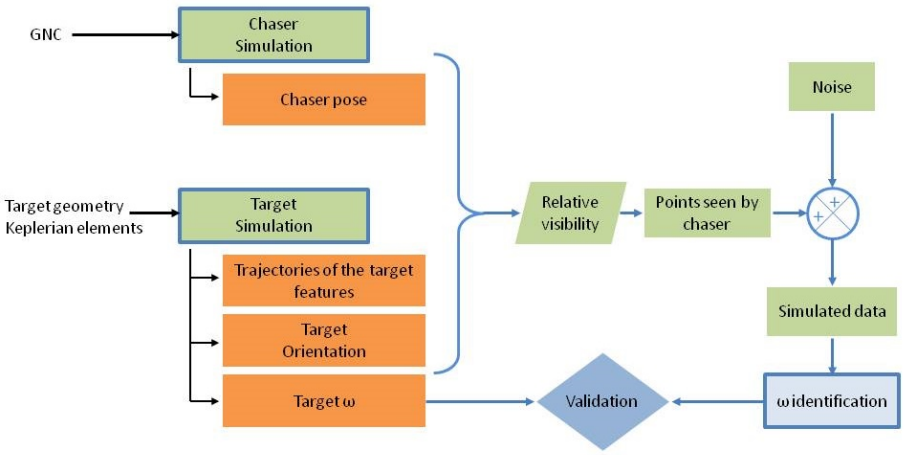

Figure 2: Flowchart describing data creation and algorithm validation.

initial inputs are the target geometry, *i.e.*, several points on the H10's surface, the Keplerian elements, and the control strategy of the chaser. Using this information, the models generate the simulated data. In addition to the trajectory of the points, these data consist of the kinematic state of the target. This information is used to validate the results of the angular velocity reconstruction. Simple equations describing the motion of an Earth artificial satellite are:

$$ {}^{I}\ddot{\bar{\rho}} = \frac{\Upsilon}{\| {}^{I}\bar{\rho}\|^3} {}^{I}\bar{\rho} + {}^{I}\bar{\mathcal{S}}_d \tag{1} $$

$$ J\, {}^{b}\dot{\bar{\omega}} + {}^{b}\bar{\omega}^{\times} J\, {}^{b}\bar{\omega} = {}^{I}\bar{\mathcal{C}}_d \tag{2} $$

In the first equation, known as the Kepler equation, ${}^{I}\bar{\rho}$ is the body mass center position in an Earth-centered inertial frame I, Υ is the planetary constant, and ${}^{I}\bar{\mathcal{S}}_d$ is the resultant of environmental forces.

Eq. 2, known as the Euler equation, contains the body rate ${}^{b}\bar{\omega}$ whose estimation is the object of this article. All of the variables in equation 2 are expressed in the body-fixed reference frame b, whose axes can be, for example, aligned with the principal axes for that body. In the remainder of the paper, we assume that the reference b will fulfill this property.

When the body is an uncontrolled object in space, such as a failed spacecraft, space debris, or something similar, ${}^b\bar{\mathcal{C}}_d$ reduces to the sum of environmental torques, which is (in general) very small, especially when J, *i.e.*, the inertia tensor, has particular forms (*e.g.*, the principal inertia tensor of an axisymmetric body has two equal elements on the diagonal).

For example, when ${}^b\bar{\mathcal{C}}_d$ is a mathematical model of the gravity gradient torque, the numerical integration of eq. 2 in a relatively short time interval shows that the components of ${}^b\bar{\omega}$ are not significantly different from those obtainable using the analytic solution of eq. 2 with ${}^b\bar{\mathcal{C}}_d = 0$ and $J_1 > J_2 > J_3$ [19]:

$$\begin{aligned} {}^b\omega_1 &= \mathcal{P}\, cn[\Xi, \Theta] \\ {}^b\omega_2 &= \mathcal{Q}\, sn[\Xi, \Theta] \\ {}^b\omega_3 &= \mathcal{R}\, dn[\Xi, \Theta] \end{aligned} \tag{3}$$

$\mathcal{P}$, $\mathcal{Q}$, $\mathcal{R}$, and Θ are constants that depend on both the initial rate and the inertia tensor; Ξ is a linear function of time; and cn, sn, and dn are the Jacobi elliptic functions.

The absolute rate $\bar{\omega}$ of a generic body expressed in a body-fixed reference frame is strictly related to the frame orientation [20], as indicated by eq.4:

$${}^b\bar{\omega} = 2(q_0\dot{\bar{q}} - \bar{q}\dot{q}_0) - 2\bar{q}^{\times}\dot{\bar{q}} \tag{4}$$

where q_0 and $\bar{q}$ are, respectively, the scalar and the vector components of the unit quaternion $\tilde{q}$. The notation $\bar{q}^{\times}$ denotes the skew-symmetric matrix:

$$\bar{q}^{\times} = \begin{bmatrix} 0 & -q_3 & q_2 \\ q_3 & 0 & -q_1 \\ -q_2 & q_1 & 0 \end{bmatrix} \tag{5}$$

where q_1, q_2, and q_3 are the components of $\bar{q}$. Quaternions are very useful for representing the orientation of a reference frame because the mapping is never singular. This property holds because of the introduction of a fourth dependent parameter, whereas only three independent parameters are sufficient to uniquely determine the orientation of the frame.

An immediate consequence of the above-mentioned property is that the mapping between quaternions and angular rate is singularity-free; therefore, eq. 4 can be conveniently rewritten as:

$$\dot{\bar{q}} = \frac{1}{2}(\bar{q}^{\times}\,{}^{b}\bar{\omega} + q_0\,{}^{b}\bar{\omega}) \qquad \wedge \qquad \dot{q_0} = -\frac{1}{2}\bar{q}^{T}\,{}^{b}\bar{\omega} \tag{6}$$

The attitude of the body, *i.e.*, the orientation of the body-fixed reference frame b in the inertial frame I, can then be represented in matrix form using the following compact formula:

$${}^{I}\mathcal{A}_{b}^{T} = \left(q_0^2 - \bar{q}^T\bar{q}\right) I_3 + 2\bar{q}\bar{q}^T - 2q_0\bar{q}^{\times} \tag{7}$$

where I_3 indicates the 3×3 identity matrix.

The matrix ${}^{I}\mathcal{A}_{b}$ belongs to the special orthogonal group of dimension 3, $SO(3)$. Knowledge of this matrix allows us to evaluate the position of any point w on the benchmark body in a chaser-fixed (observer) frame ch with its origin on the simulated chaser spacecraft:

$${}^{ch}\bar{\rho}_w = {}^{ch}\mathcal{A}_I({}^{I}\bar{\rho} + {}^{I}\mathcal{A}_b\bar{d}_w) + {}^{ch}\bar{p}_I + \bar{\eta} \tag{8}$$

where $\bar{d}_w$ is the position of the w-th point relative to center of mass in the body-fixed reference frame, ${}^{ch}\bar{p}_I$ is the position of the origin of the inertial frame in the observer frame (i.e., the position of the Earth's center from the observer's point of view), ${}^{ch}\bar{\rho}_w$ is the position of the w-th point in the observer frame, and $\bar{\eta}$ is white Gaussian noise representing uncertainty in the coordinates measured by the stereo-vision sensor.

Eq. 8 allows the calculation of a data set that could be used as an input for the rate estimation algorithm. However, the availability of a series of point coordinates at equidistant time instants cannot be assumed. In fact, it is easily to assume that, in a specific time window, a certain number of features of the body are completely hidden from the observer. This situation occurs whenever the observer cannot perform flybys of the body.

Therefore, even without considering occlusions, if the body has only a small number of features, *e.g.*, four or five, there might be several time windows in

which no information about the attitude is available, meaning fewer than three points might be visible (at a given time) to the observer.

A back-face culling [21] algorithm can be applied to identify the time instants

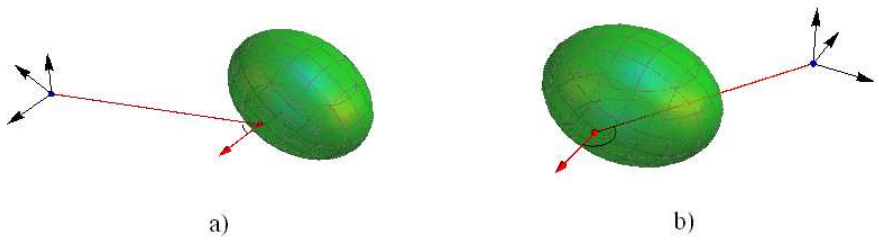

Figure 3: Illustration of the main back-face culling rule: a) visible point; b) hidden point

in which a generic point w is not observable.

In brief, the back-face culling algorithm consists of the evaluation of the angle formed by the observation direction and the normal to the surface containing the observed point. If the angle is acute, the point is visible. Fig. 3 provides an illustration of the aforementioned rule: the triad of axes is representative of the observer; cases a) and b) show a visible point and a hidden point, respectively. Using the above algorithm, it is possible to create a Boolean array χ_w for the generic point w containing the visibility information. However, when the body is not convex, this method does not produce reliable results. Many complex solutions [21] are available in the literature; they provide precise simulations with bodies of any shape. For the purposes of this paper, however, coarse evaluation of the occlusion period is sufficient.

According to the array χ_w, the attitude of the space debris, represented by quaternions, must be calculated from the available trajectories of a group of points, expressed as a time-series of Euclidean coordinates. Calculation is possible whenever at least three triplets of coordinates of non-aligned points of the benchmark body are available.

Given three different points in $\mathbb{R}^3$ belonging to a rigid body, one can define two column vectors, $\bar{v}_i$ and $\bar{v}_u$, whose cross product is the vector $\bar{v}_j$, which is perpendicular to both. A third column vector, $\bar{v}_k$, can be simply obtained through

another cross product between $\bar{v}_i$ and $\bar{v}_j$. Then, the orientation of a body-fixed reference frame $\mathcal{F}$, which (in general) is different from the b reference frame, with respect to the inertial frame I, is given by the following expression:

$$ {}^{I}\mathcal{A}_{\mathcal{F}} = \left[\begin{array}{ccc} \hat{v_i} & \hat{v_j} & \hat{v_k} \end{array} \right] \in SO(3) \tag{9} $$

Vectors $\hat{v_i}$, $\hat{v_j}$, and $\hat{v_k}$ are the unit vectors corresponding to $\bar{v_i}$, $\bar{v_j}$, and $\bar{v_k}$, respectively. As mentioned above, a non-singular mapping between an element of the $SO(3)$ group and a unit quaternion always exists; one of the four possible ways to calculate the quaternion is as follows:

$$ \tilde{q} = \left[\begin{array}{c} \pm\frac{1}{2}\sqrt{1 + A_{11} + A_{22} + A_{33}} \\ \frac{1}{4q_0}(A_{32} - A_{23}) \\ \frac{1}{4q_0}(A_{13} - A_{31}) \\ \frac{1}{4q_0}(A_{21} - A_{12}) \end{array} \right] \tag{10} $$

Eq. 10, in which A_{ij} is an element of matrix ${}^{\mathcal{F}}\mathcal{A}_I$ (the inverse of ${}^{I}\mathcal{A}_{\mathcal{F}}$), provides evidence that the quaternion $-\tilde{q}$ represents the same orientation as $\tilde{q}$. This property allows this representation to be singularity-free; however, the calculation process requires that more than one choice be made. This requirement means that describing the evolution of the attitude of a body with four time-continuous parameters is not trivial. Several algorithms can be developed to calculate quaternions $\tilde{q}(t_k)$ that can be interpolated using continuous curves for a given temporal sequence of rotation matrices ${}^{I}\mathcal{A}_{\mathcal{F}}(t_k)$.

For example, an effective algorithm can be composed of the following steps:

1. calculate four quaternion components as a function of the elements of the principal diagonal of ${}^{I}\mathcal{A}_{\mathcal{F}}(t_k)$ (*e.g.,* q_0 in eq. 10);
2. evaluate the maximum value q_{max}, and then, calculate $\tilde{q}(t_k)$ according to $q_h = q_{max}$ (a good example is again given by eq. 10 with $q_h = q_0$);
3. apply the following rule to guarantee continuity (except when $k = 0$):

$$ \text{if} \qquad q_h(t_{k-1}) < 0 \qquad \text{then} \qquad \bar{q}(t_k) \leftarrow -\bar{q}(t_k) $$

Note that this kind of algorithm fails when the time step is not constant; therefore, if there is any lack of information at some time instant regarding the attitude of the body, the continuity of the quaternions cannot be guaranteed.

Another problem that occurs is that for two distinct instants, the observer will (in general) see different features of the objects; thus, it is necessary to assume complete knowledge of all transformation matrices (constant) between all possible body-fixed reference frames $\mathcal{F}$ whose orientations with respect to I can be evaluated via eq. 9.

The above assumption coincides with assuming knowledge of the relative positions between all features, as the orientations of the body-fixed frames depend on only these positions. If the number of features is $\mathcal{B}$, the number of all possible body-fixed reference frames is $\binom{\mathcal{B}}{3}$. When at least three features are observable,

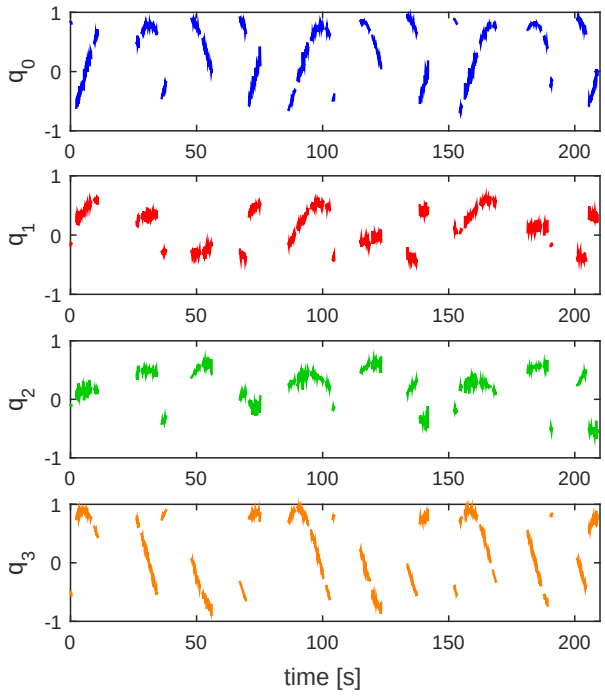

Figure 4: Raw attitude information

the orientation ${}^{\mathcal{F}^*}\mathcal{A}_I$ of one specific frame $\mathcal{F}^*$ can be obtained through the above mentioned transformation matrices; the associated quaternion can also be obtained using eq. 10. These methods consider feature visibility, which, combined with coordinates calculated using eq. 8, are useful for calculating parts of time-series of noisy quaternions. However, these time-series cannot be interpolated using a unique continuous curve that correctly describes the evolution of the orientation of the body.

One example of the result of the evaluation of realistic attitude data is shown in fig. 4: quaternion signals refer to the chosen benchmark body assumed at an initial time ${}^b\bar{\omega}_0 = [10.2 \quad 0.72 \quad -17.1]$ deg/s. The normalized vector of the three principal moments of inertia has been set to $\bar{J} = [0.7014 \quad 0.5762 \quad 0.4196]$; note that the magnitude of the aforementioned vector does not influence the solution of eq. 2. White Gaussian noise with zero mean and a standard deviation of 3 cm was added to the Euclidean coordinates of the benchmark's features. In fig. 4, a noisy $4 \times m$ signal is illustrated; however, for each m-dimensional component, only a number, p, of samples are real numbers. A number, $m-p$, of samples are missing because of deficient detection of the features of the benchmark (fewer than three features are detectable).

The restoration of the complete signal $\tilde{q} \in \mathbb{R}^{4\times m}$ can be split into the parallel recovery of the time series of each quaternion component. Then, typical compressed sensing techniques can be adopted to recover the four corrupted signals.

3. Basis pursuit and SALSA algorithm

In general, a noisy measured signal with missing samples $s \in \mathbb{R}^p$ can be modeled as:

$$s = H\sigma + \eta \tag{11}$$

where $\sigma \in \mathbb{R}^m$ represents the unknown original signal, η represents the noise, and H is a $p \times m$ matrix that can be defined using the following expression:

$$H^T H = \mathrm{diag}(\tau) \tag{12}$$

where τ is an array whose elements τ_j, $j = 1, 2..., m$ are equal to zero when a lack of attitude information is associated with the time instant t_j. Otherwise, τ_j is equal to one. Using these definitions, we find that H must be a matrix whose columns are null when the column index corresponds to a time instant with a lack of attitude information. Additionally, it is easy to verify that the following equation holds, $HH^T = I_p$, where I_p is the $p \times p$ identity matrix.

The theory of compressed sensing addresses the problem of recovering a signal that is approximately decomposable into a linear combination of a small number of elementary functions of time. Given a large set of functions, a finite number of unit-norm signals, which are also called *atoms*, can be derived. Then, signal recovery consists in finding the smallest number of atoms whose linear combination optimally fits the available measurements of the signal. All of the atoms are grouped into a set that is called a *dictionary*. The dictionary synthesis matrix Φ is defined as a representation of the linear mapping between certain complex coefficients $c \in \mathbb{C}^n$ and the original signal σ. An interesting dictionary is the so-called *Fourier dictionary*; the synthesis matrix Φ of this dictionary is given by the following formula:

$$\sigma_k = \sum_{u=0}^{n-1} c(u) e^{i\frac{2\pi}{n}uk} \qquad \forall k = 0, 1, ..., m-1 \tag{13}$$

$$\Phi_{k,u} = e^{i\frac{2\pi}{n}uk} \quad \forall k = 0, 1, ..., m-1 \quad \wedge \quad \forall u = 0, 1, ..., n-1 \tag{14}$$

When m is equal to n, the linear mapping $\Phi : \mathbb{C}^n \to \mathbb{R}^m$ becomes the so-called inverse discrete Fourier transform (IDFT) multiplied by the normalization constant n. Additionally, it is possible to define the dictionary analysis matrix Φ^* as the conjugate-transpose of Φ, showing that when $m = n$ the linear mapping $\Phi^* : \mathbb{R}^m \to \mathbb{C}^n$ becomes the so-called discrete Fourier transform (DFT). This property holds because of the orthogonality of the matrix Φ. We define the *coherence* parameter as follows:

$$\vartheta = \max_{\iota \neq \kappa} \left| \sum_{k=0}^{m-1} \Phi_{k,\iota} \Phi_{k,\kappa} \right| \tag{15}$$

where the Fourier dictionary is found to be completely incoherent ($\vartheta = 0$). Coherence is a useful property for a dictionary because it is a measure of the linear independence of the atoms; intuitively, signal recovery is easier if the atoms are all orthogonal.

Based on these definitions, eq. 11 can be conveniently rewritten as:

$$s = H\Phi c + \eta = \tilde{\Phi} c + \eta \tag{16}$$

Eq. 16 proposes the problem of estimating the coefficient vector c from a noisy signal with missing samples s. A problem that is optimal to recover the signal could be stated as follows:

$$\arg\min_{c} \|c\|_0 \qquad \text{subject to} \qquad \|s - \tilde{\Phi} c\|_2 \leq \varepsilon_0 \tag{17}$$

where ε_0 is a reasonable tolerance of the estimation error and the $l0$-norm is defined as the number of non-zero elements of the argument. Unfortunately, obtaining a solution to this problem requires searching for a solution among all possible combinations of the non-zero elements of c. For this reason, it is appropriate to use a relaxation of the problem, which leads to the following problem:

$$\arg\min_{c} \|c\|_1 \qquad \text{subject to} \qquad \|s - \tilde{\Phi} c\|_2 \leq \varepsilon_1 \tag{18}$$

where ε_1 depends on ε_0 and the $l1$-norm is defined as the sum of the elements of the argument. Note that the problem in eq. 18 is convex; thus, it has only one suitable solution, if a solution exists. However, a more convenient method to solve this problem is to write it in its Lagrangian form:

$$\arg\min_{c} \frac{1}{2} \|\tilde{\Phi} c - s\|_2^2 + \lambda \|c\|_1 \tag{19}$$

The regularization parameter λ depends on ε_1; it is defined as a *penalization parameter*: when λ is equal to zero, the entire noise vector will be preserved and contained in the found coefficients. For higher values of λ, the signal will be smoother but the recovery will be less accurate.

The problem stated in eq. 18 is known as the *basis pursuit denoising* problem,

while the one stated in eq. 19 is known as the *lasso* problem.

After re-normalization of the columns, the dictionary associated with the synthesis matrix $\tilde{\Phi}$ has a non-null coherence ϑ. However, the condition of having a null coherence is not mandatory: as stated in [22], the fundamental condition that assures that an exactly sparse signal can be optimally recovered with most of the existing algorithms is that the *exact recovery coefficient ERC* is greater than 0. The *ERC* defines the extent to which a subset of linearly independent atoms in a dictionary is different from any other subset in it. Thus, altought the coherence is not null, it is sufficient that the signal can be represented as a combination of atoms that are not too similar to others in the dictionary.

Therefore, the dictionary associated to $\tilde{\Phi}$ was chosen for the recovery of quaternions. It has been found that the sparsity of the original signal to be recovered is an important property if the basis pursuit is to be the most efficient strategy for signal recovery. It is difficult to demonstrate that the quaternions' component signals have a sparse frequency spectrum. Eq. 3 and eq. 6 show that (in general) the quaternion components should not be *exactly* sparse; however, they should have very few frequency components that have a significant amplitude. Numerical simulation confirms this statement if quaternions represent the orientation of a body free from external torques [23].

The algorithm chosen by the authors to solve the problem in eq. 19 is an adapted version of the so-called split augmented Lagrangian shrinkage algorithm, which is also known by its acronym, SALSA [17]. The two most important theoretical contributions to the algorithm are so-called variable splitting and the use of the augmented Lagrangian function. Variable splitting simply consists of introducing a new variable $v = c$ in the optimization problem. On the other hand, the second contribution of SALSA consists of introducing in the Lagrangian formulation of the problem an extra weight to the constraint $v - c = 0$.

The application of these two contributions leads to the following formulation of the problem:

$$\arg\min_{c,v} \frac{1}{2}\|\tilde{\Phi}c - s\|_2^2 + \lambda\|v\|_1 + \frac{\mu}{2}\|c - v - l\|_2^2 \tag{20}$$

where $\mu \geq 0$ is another penalization parameter and l is an appropriate constant value.

In this formulation of the problem, the high value of the parameter μ forces the equality of c and v, compensating for the introduction of a new auxiliary variable. However, the problem in eq. 20 is difficult to solve because both variables, c and v, are in the norm. One way to address this issue is to minimize the function for only one variable while holding the other fixed; this is repeated alternately for the two variables for a fixed number of iterations. This algorithm is the proposed SALSA algorithm. The algorithm consists of the following operations once λ, μ, and some arbitrary initial guesses v_0 and l_0 are chosen:

- $c_{\nu+1} = \arg\min_c \|\tilde{\Phi}c - s\|_2^2 + \mu\|c - v_\nu - l_\nu\|_2^2$
- $v_{\nu+1} = \arg\min_v \lambda\|v\|_1 + \frac{\mu}{2}\|c_{\nu+1} - v - l_\nu\|_2^2$
- $l_{\nu+1} = l_\nu - (c_{\nu+1} - v_{\nu+1})$
- $\nu \leftarrow \nu + 1$

These basic steps can be solved in a closed form: the first step represents a classic constrained least-squares optimization problem, as the function to be minimized is a strictly convex quadratic function. The solution is as follows:

$$c_{\nu+1} = (\tilde{\Phi}^*\tilde{\Phi} + \mu I_n)^{-1}(\tilde{\Phi}^* s + \mu(v_\nu + l_\nu)) \tag{21}$$

The second step is minimization of a function that is a pure denoising function, meaning that the parameter λ is the regularizer of the equivalence condition between a known vector $c_{\nu+1} - l_\nu$ and the variable v: if $\lambda = 0$, $v = c_{\nu+1} - l_\nu$; if λ is bigger than zero, it induces sparsity in v. The closed-form solution to this kind of problem is well known [24]. Specifically, when the regularizer is applied to the $l1$-norm, the solution is the so-called *soft-thresholding function*.

Then, the solution to the second step is:

$$v_{\nu+1} = \text{soft}\left(c_{\nu+1} - l_\nu, \frac{\lambda}{\mu}\right) \tag{22}$$

To obtain a simpler algorithm, this method can be slightly modified, according to [25], by changing the variables $u_\nu = v_\nu + l_\nu$. Thus, eq. 21 can be written as follows:

$$c_{\nu+1} = (\tilde{\Phi}^*\tilde{\Phi} + \mu I_n)^{-1}(\tilde{\Phi}^* s + \mu u_\nu) \tag{23}$$

Using the matrix-inverse lemma, and the following properties:

$$HH^T = I_p \tag{24}$$

$$\tilde{\Phi}\tilde{\Phi}^* = nI_p \tag{25}$$

the expression 23 can be turned into

$$c_{\nu+1} = \left(\frac{1}{\mu} I_n - \frac{1}{\mu(\mu+n)}\tilde{\Phi}^*\tilde{\Phi}\right)(\tilde{\Phi}^* s + \mu u_\nu) = u_\nu + \frac{1}{\mu+n}\tilde{\Phi}^*(s - \tilde{\Phi} u_\nu) \tag{26}$$

which leads to:

$$c_{\nu+1} = u_\nu + \frac{1}{\mu+n}\Phi^*[H^T s - \mathrm{diag}(\tau)\Phi u_\nu] \tag{27}$$

This equation shows that because a fast transform that maps coefficients to signals and vice-versa exists (*i.e.*, the direct and inverse fast Fourier transform), the explicit computation of Φ and Φ^* can be avoided, which allows the algorithm to be very fast and efficient.

Then, the final algorithm obtained (gathering all of the equations presented in this section) is a follows:

- $u_{\nu+1} = \mathrm{soft}(c_\nu - l_\nu, \lambda/\mu) + l_\nu$
- $c_{\nu+1} = u_\nu + \frac{1}{\mu+n}\Phi^*[H^T s - \mathrm{diag}(\tau)\Phi u_\nu]$
- $l_{\nu+1} = u_{\nu+1} - c_{\nu+1}$
- $\nu \leftarrow \nu + 1$

To implement the algorithm, it is still necessary to choose values for λ and μ, and to specify the initial guesses for c_0 and l_0.

4. Attitude recovery

Eq. 10 shows that the two opposite quaternions represent the same attitude of a body. Therefore, the methods described in the previous sections are not directly applicable to recovery of quaternion signals (such as those represented in fig. 4).

Actually, the recovery of the missing samples for these kinds of signals does not, in general, lead to the recovery of a continuous attitude signal. In fact, once the sign of the first value of the quaternions is chosen, the signs of the other (subsequent) values are not freely selectable: when the signs are randomly selected, the attitude signal, in general, presents abrupt changes. However, having fixed the sign for the first value, a unique sequence of choices that leads to a smooth signal exists. In other words, the assumption concerning the sparsity of the quaternions is valid only if the sign of each value of the quaternions is properly selected. This selection is often made by exploiting known algorithms, an example of which was presented in section 2. Unfortunately, these algorithms are not applicable when the quaternions have missing samples.

One approach to this problem consists of recovering all possible signals produced by all possible choices of value signs of the signals. This principle is based on the hope of finding some criterion to identify the unique smooth signal that represents the body attitude.

The quaternion signals that have missing samples can be considered a set of N pieces. Excluding the first piece, all of the other pieces may be marked with a Boolean label. If no changes have been made to the sign of the values of the input pieces, all of the labels are set to zero. On the contrary, whenever a sign change is applied to the values of a specific piece, the Boolean label switches to one. Thus, by sorting all the $N-1$ digits, a set of labels that uniquely characterizes the relationship between a generic sequence and the original input sequence can be composed.

Based on these considerations, note that the number of all possible different signals must be 2^{N-1}. These signals contain the same piece of information re-

garding the attitude of the body.

Once all of the signals have been recovered, we must determine which criterion can be used to identify the correct signal.

For example, we can assume that the searched signal is the *sparsest* signal from among the recovered signals. This assumption is supported by numerical simulations. In particular, when changing the initial conditions of the benchmark debris, the quaternions are always very sparse. Furthermore, it is intuitive that signals with abrupt variations have a more complex frequency spectrum than smooth signals. Clearly, if the noise has a large amplitude, the quaternions are not more sparse; however, in this case, it seems impossible to separate the attitude information from the noise using any method.

The sparsity of the h-th signal can be quantified using, for example, a penalty score calculated as follows:

$$PS = const_1 \|c_h\|_0 + const_2 \|c_h\|_1 \tag{28}$$

where $const_1$ and $const_2$ are two constant gains, and c_h is the vector of the coefficients of the Fourier transform of the recovered h-th signal. Any reasonable score can be used to make classifications of the signals. The score used herein has been proven to be valid using numerical simulations.

Using this principle, we find that if the number N of pieces of quaternions is large, the total number of piece-wise signals that should be recovered would increase exponentially, which would make the explained idea inapplicable. For example, the quaternions shown in fig. 4 present a number of pieces $N = 28$ for each element, which means that the overall number of signals that should be recovered would be roughly one hundred million.

A good method for making the recovery procedure feasible consists of preliminarily considering a relatively small number $N' << N$ of pieces, and then, recovering all of the resulting $2^{N'-1}$ signals. This technique allows us to make a preliminary selection of the best signals. Once one or more signals are selected using the score in eq. 28, complete recovery is performed by adding new pieces with both possible signs. Specifically, every intermediate recovery is followed by

discarding the worst recovered signals. At the end of this procedure, only the best signal remains.

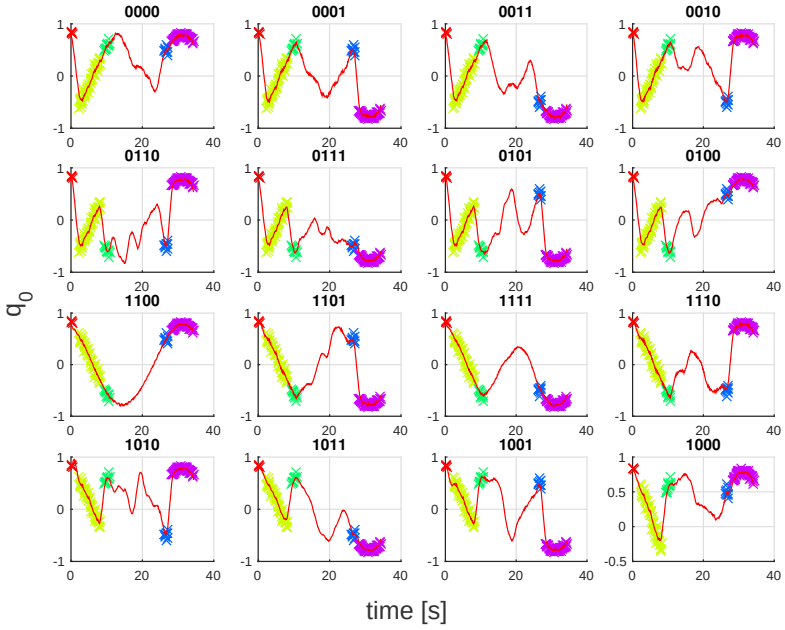

Figure 5: Preliminary phase, $N' = 5$: raw data (crosses) and recovered signal (red line)

Considering the quaternions shown in fig. 4, a number $N' = 5$ pieces of q_0 is considered. Note that the number N' cannot be excessively low because deficient information in terms of measurements leads to poor preliminary recovery. In fig. 5 recovery for sixteen signals is shown. Each signal is characterized by a set of boolean labels that specifies the relationship between the signal itself and the original input, marked with 0000.

In fig. 6, a bar chart showing the penalty scores for the recovered signals is presented. Intuitively, the sparsest recovered signals are those marked with 1100 and 1111 (see also fig. 5). However, it is difficult to predict which of the two signals is actually the best. Therefore, they are both preserved for the next phase, in which the 6-th piece of q_0 is added to the two best recovered signals (see fig. 7 for an example).

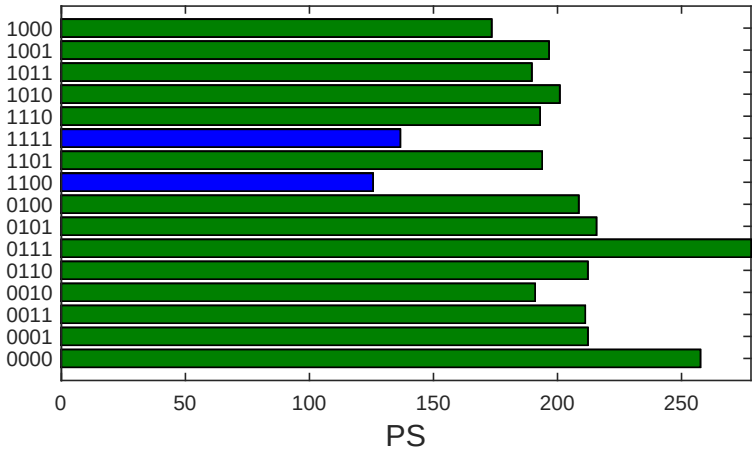

Figure 6: Values of penalty scores; best recoveries in blue correspond to 1111 and 1100 label sets

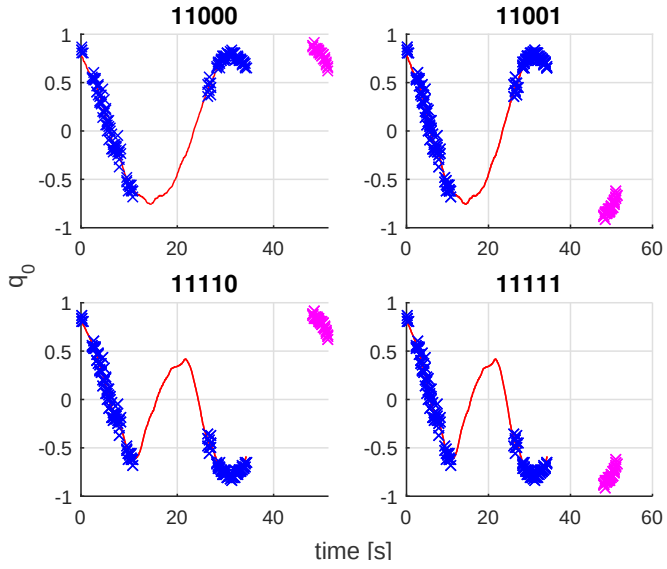

Figure 7: Introduction of a new piece of quaternion: the component is added to the best recovered signals with opposite sign

The new signals could be recovered using the same method as used in the preliminary phase. Therefore, a new score calculated using eq. 28 can be associated

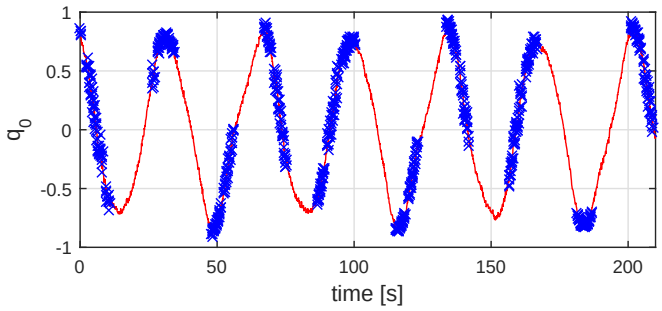

Figure 8: Final best recovery of the quaternion: raw data (blue crosses) and recovered signal (red line)

485 with each recovered sequence so as to eliminate the worst cases. This process can be stopped when all of the available input data are exploited. The complete recovered q_0 signal is shown in fig. 8.

Fig. 9 presents the complete recovery of four different quaternion signals derived

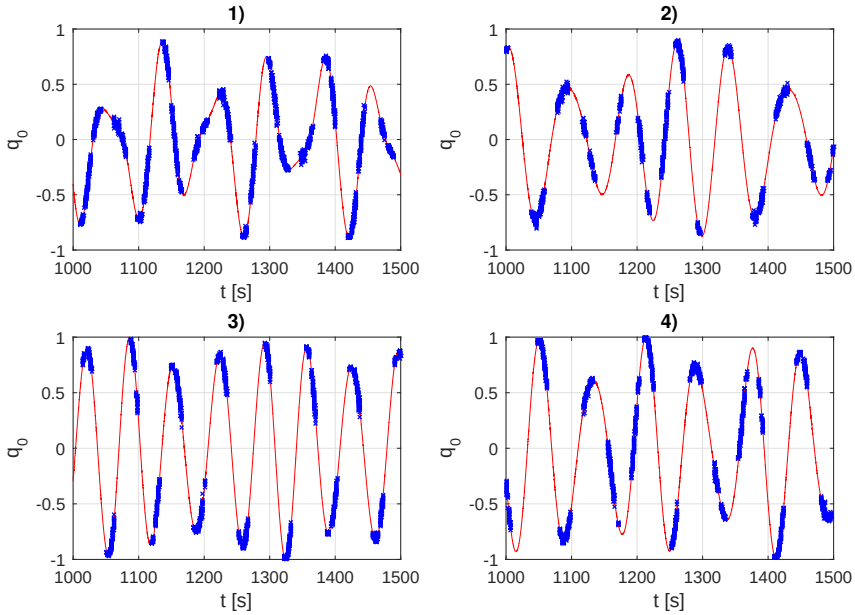

Figure 9: Attitude recovery performed for different benchmark conditions (see tab. 1).

CaseID	J_1	J_2	J_3	ω_{01}	ω_{02}	ω_{03}	ε_θ
1)	0.618	0.707	0.345	7.200	5.525	-1.624	0.507
2)	0.601	0.446	0.664	8.400	-0.263	2.860	0.520
3)	0.657	0.489	0.574	7.200	5.914	6.023	0.712
4)	0.518	0.461	0.720	6.000	6.600	4.440	0.582
M. unit:	[ ]	[ ]	[ ]	[deg/s]	[deg/s]	[deg/s]	[deg]

Table 1: pitch angle error for different conditions of the benchmark (algorithm's output in fig. 9); standard deviation of the measurement noise is equal to 5 cm

from distinct sets of initial angular rates and inertial properties of the benchmark spacecraft. The benchmark motion simulation has been run for 1500 s. Only the final parts of the signals are shown ir order to better illustrate the output quality. For these cases the standard deviation of the noise added to the feature coordinates has been increased to 5 cm.

The conditions of each of the cases are listed in tab. 1. The latter table presents also root-mean-square errors (RMSE) for each attitude recovery in terms of the corresponding ZYX Euler angles (error in the pitch angle: ε_θ). Table. 2 illustrates the RMSE for other six different recoveries. The outputs relative to these last scenarios are not shown as they do not provide remarkable information for a deeper understanding of the algorithm capabilities.

From a brief analysis of the data presented in tab 1 and in tab 2 it appears that errors are in the order of $5 \cdot 10^{-1}$ deg for pitch angles. In particular, the mean value of RMSE in the considered cases is equal to 0.611 deg, while the error range is from 0.506 deg to 0.813 deg

Making for instance a comparison with the method presented in [10] which, altought is a very effective method, is not fault-tolerant, the errors made in estimating attitude are comparable. In [10], the noise added to the feature coordinates is dependent by the distance between chaser and target along the direction of the focal axes of the cameras. Indeed, the noise is added at pixel level. Multiplying the amplitude of this noise for a reference value of the afore-

CaseID	J_1	J_2	J_3	ω_{01}	ω_{02}	ω_{03}	ε_θ
5)	0.295	0.781	0.551	7.200	0.253	-13.198	0.612
6)	0.531	0.473	0.703	8.400	0.545	0.458	0.597
7)	0.719	0.658	0.224	6.600	1.296	9.557	0.513
8)	0.745	0.512	0.427	6.000	-7.620	12.000	0.567
9)	0.742	0.521	0.421	-3.000	4.800	-2.700	0.814
10)	0.371	0.743	0.557	3.000	-4.800	-2.100	0.566
M. unit:	[ ]	[ ]	[ ]	[deg/s]	[deg/s]	[deg/s]	[deg]

Table 2: pitch angle error for different conditions of the benchmark; standard deviation of the measurement noise is equal to 5 cm

mentioned distance we can roughly obtain an idea of the corresponding order of magnitude of the noise at coordinate level. Considering 10^{-4} of noise amplitude at pixel level, which coarsely corresponds to 1 cm for a distance of 100 m, the estimation method in [10] produces errors in pitch angle that are under 2.5 deg (90th percentile). Considering instead 10^{-5} of noise amplitude at pixel level, which corresponds approximately to 1 mm for a distance of 100 m, the obtained error decreases to $2 \cdot 10^{-1}$ deg (90th percentile).

On the other hand, the attitude recovery method proposed in this paper produces errors (without Kalman filtering) in the pitch angle that are in the order of $5 \cdot 10^{-1}$ deg, having 5 cm of noise amplitude at coordinate level. After a comparison with the current state of the art, this result is quite encouraging with a view on future practical applications of this method.

Finally, certain considerations regarding the sample period should be made: the value strictly depends on the type of sensor chosen for tracking the features of the body. The recovery is reliable if the sampling frequency is sufficiently higher than the highest significant frequency in the quaternion signal. Fortunately, most torque-free space bodies have a slowly oscillating attitude; thus, tracking sensors such as simple cameras often have a high acquisition frequency. For example, a sampling frequency equal to $1Hz$ is considered sufficient.

5. Angular rate estimation

The estimation of the rate from attitude information, *i.e.*, from eq. 4, requires the evaluation of the quaternion's derivative. Numerically performing the derivative of the estimated signal produces unacceptable results because the recovered attitude signal still contains high frequency noise, which is drastically amplified in the numerical derivative. To solve this issue, an unscented Kalman filter (UKF) was implemented. The discrete-time nonlinear dynamic system,

$$x_{t+1} = f\left(x_t\right) + \theta_t = x_t + \Delta t \begin{bmatrix} \frac{1}{2}\Omega\left({}^{b}\bar{\omega}_t\right){}^{b}\tilde{q}_t \\ 0_{3\times 1} \\ \operatorname{diag}\left(\bar{J}_t\right)^{-1}\left[{}^{b}\bar{\omega}_t \times \left(\operatorname{diag}\left(\bar{J}_t\right){}^{b}\bar{\omega}_t\right)\right] \\ 0_{3\times 1} \end{bmatrix} + \theta_t \quad (29)$$

$$y_t = h\left(x_t\right) + e_t = {}^{b}\tilde{q}_t \otimes {}^{o}\tilde{q}_t + e_t \quad (30)$$

served as framework for the UKF. In eq. 29 the state vector $x_t = \left[{}^{b}\tilde{q}_t \;\; {}^{o}\tilde{q}_t \;\; {}^{b}\bar{\omega}_t \;\; \bar{J}_t\right]^T$ contains: the unit quaternion ${}^{b}\tilde{q}$ that describes the attitude between a principal body frame b and the inertial frame I; the offset quaternion ${}^{o}\tilde{q}$ that describes the attitude between a generic body frame $\mathcal{F}$ and b; ${}^{b}\bar{\omega}$ the angular velocity of the body frame with respect to b; the column array $\bar{J}$ which entries are the normalized principal moments of inertia of the target body. Moreover, Δt indicates the time step.

$$\Omega\left({}^{b}\bar{\omega}_k\right) = \begin{bmatrix} 0 & -{}^{b}\omega_1 & -{}^{b}\omega_2 & -{}^{b}\omega_3 \\ {}^{b}\omega_1 & 0 & {}^{b}\omega_3 & -{}^{b}\omega_2 \\ {}^{b}\omega_2 & -{}^{b}\omega_3 & 0 & {}^{b}\omega_1 \\ {}^{b}\omega_3 & {}^{b}\omega_2 & -{}^{b}\omega_1 & 0 \end{bmatrix} \quad (31)$$

$\Omega\left({}^{b}\bar{\omega}_k\right)$ is a skew-symmetric matrix (see eq. 31) and θ_t is the process noise. Regarding eq. 30, $y_t = \tilde{q}_t$ is the measurement vector, the operator $\otimes$ represents the quaternion multiplication, and e_t is the measurement noise. This equation states that the attitude of a generic body frame $\mathcal{F}$ may be expressed as the concatenation of the attitude of the body frame b plus a constant offset quaternion.

The UKF at first generates a set of points called sigma points. These sigma points are created exploiting the unscented transformation which is a method for calculating the statistics of a random variable which undergoes a non linear transformation [26] [27]. The application of the UKF may be performed as follows:

Calculate sigma points:

$$X_t = [\hat{x}_t \ \dots \ \hat{x}_t] + \sqrt{\alpha}\left[0_{14\times 1} \ \sqrt{P_t} \ -\sqrt{P_t}\right] \tag{32}$$

Prediction:

$$X^-_{t+1} = f(X_t) \tag{33}$$
$$\hat{x}^-_{t+1} = \hat{X}_{t+1} w_m \tag{34}$$
$$P^-_{k+1} = \hat{X}_{t+1} W \left[\hat{X}_{t+1}\right]^T + Q_t \tag{35}$$

Update:

$$Y^-_{t+1} = h\left(X^-_{t+1}\right) \tag{36}$$
$$\hat{y}^-_{t+1} = Y^-_{t+1} w_m \tag{37}$$
$$S_{t+1} = Y^-_{t+1} W \left[Y^-_{t+1}\right]^T + R_t \tag{38}$$
$$C_{t+1} = X^-_{t+1} W \left[Y^-_{t+1}\right] \tag{39}$$

Computation of the Kalman gain:

$$K_{t+1} = C_{t+1} S^{-1}_{t+1} \tag{40}$$
$$\hat{x}_{t+1} = \hat{x}^-_{t+1} + K_{t+1}\left(y_{t+1} - \hat{y}^-_{t+1}\right) \tag{41}$$
$$P_{k+1} = P^-_{k+1} - K_{t+1} S_{t+1} K^T_{t+1} \tag{42}$$

where α is a constant that takes into account scaling parameters and adjusts the spread of the sigma points while w_m and W are respectively a vector and a matrix of weights associated with the points. P represents the state covariance matrix, Q the process noise covariance matrix and R represents the measurement noise covariance matrix. In this case at each completion of the so-called

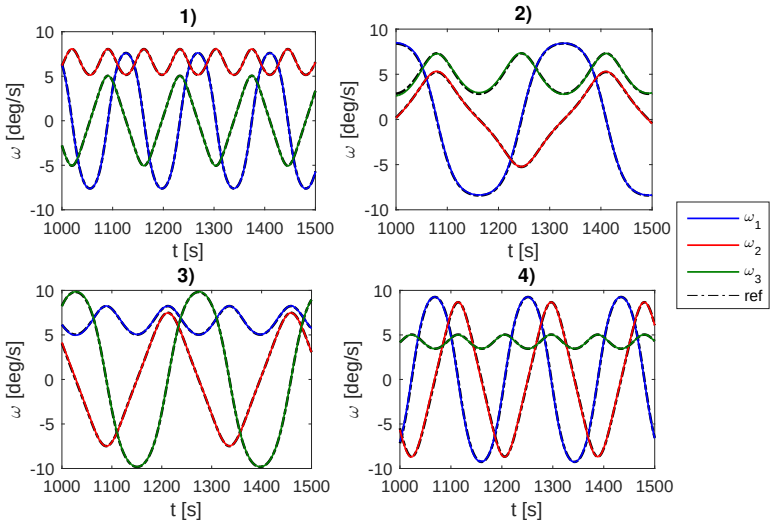

Figure 10: Final estimation of the angular rate after Kalman filtering the recovered quaternions in fig 9. Reference values of the angular rate components are represented with dashed lines

.

Kalman loop the principal moments of inertia are normalized as well as the quaternions involved. This brute-force approach is not an optimal one but is proven to work generally well [28] [29].

An example of the final result of Kalman filtering the surrogate quaternion measurements is depicted in fig. 10: the components of the estimated angular rate are compared to the ones obtained via simulation of the benchmark (see section 2).

The four shown results refer to the benchmark conditions listed in tab. 1. The estimation algorithm has been also applied to the other recovered quaternions corresponding to benchmark conditions listed in tab. 2. To show the performances of the whole approach, the final RMSE relative to each component of the estimated rate and pitch angle (after Kalman filter convergence) are listed in tab 3. Analyzing the data shown in tab. 3 it appears that the errors in the angular rate estimation are approximately between 10^{-2} deg/s and 10^{-1} deg/s.

CaseID	ε_{ω_1}	ε_{ω_2}	ε_{ω_3}	ε_{θ}
1)	0.029	0.015	0.019	0.261
2)	0.080	0.036	0.098	0.244
3)	0.032	0.045	0.036	0.398
4)	0.093	0.085	0.016	0.144
5)	0.048	0.092	0.118	0.374
6)	0.053	0.099	0.036	0.495
7)	0.016	0.015	0.048	0.194
8)	0.017	0.041	0.051	0.238
9)	0.030	0.038	0.041	0.576
10)	0.008	0.016	0.065	0.173
M. unit:	[deg/s]	[deg/s]	[deg/s]	[deg]

Table 3: angular rate and pitch angle estimation error after Kalman filtering; standard deviation of the measurement noise is equal to 5 cm

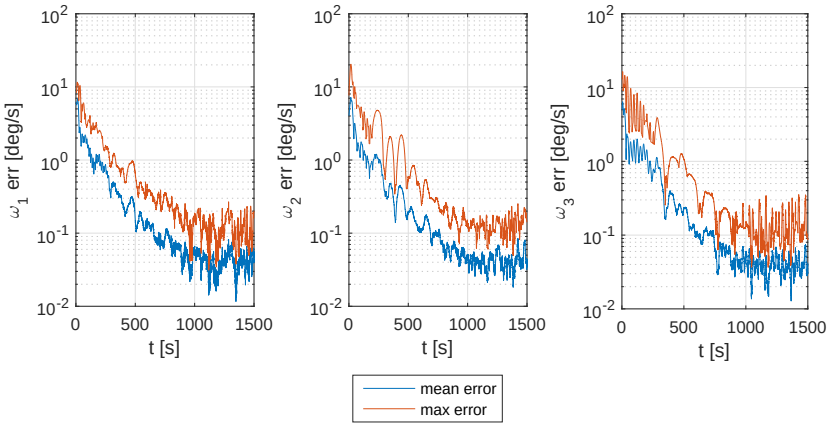

Figure 11: Mean and maximum estimation error for each angular rate component

.

Thus, the results obtained with the presented algorithm are again comparable with the results obtained in [10]. In that work the angular rate estimation error has been assessed between 10^{-2} deg/s and 10^{-1} deg/s. However, these values have been obtained starting from data affected by the minimum considered noise amplitude (10^{-5} at pixel level). In the presented work a large 5 cm noise amplitude has been considered at coordinate level.

From tab. 3, a new mean value of the error in pitch angle estimation has been evaluated (0.3 deg). As expected, the attitude estimation accuracy has been furtherly improved after the non-linear Kalman filtering stage.

Finally, to show the convergence properties of the designed unscented Kalman filter, the time behavior of mean and maximum angular rate estimation error (in the ten considered scenarios) is illustrated in fig. 11. From fig. 11, it can be noted that the error level stabilizes at about 1000 s.

6. Conclusions

A method to recover the attitude and the angular rate of an uncooperative spacecraft, or, more generally, of a space rigid body has been developed using the trajectories of several features of the object. Trajectories must be identified using stereo-vision sensors placed on a chaser spacecraft. It is not necessary that trajectories be captured at a constant sampling frequency; however, a finite number of time windows in which the sample frequency is constant must exist. Piecewise signals containing partial and corrupted information regarding the attitude of the target body can be recovered using an algorithm that exploits optimization techniques. There are no stereo-vision based methods in the current state of the art that are able to efficiently perform this recovery during occlusion periods (no measurements available). The recovery of sparse signals in the presence of Gaussian measurement noise has been successfully performed using a basis pursuit denoising approach.

The use of an unscented Kalman filter allows accurate estimation of the angular rate of the studied object starting from a complete recovered attitude signal.

The accuracy of the final results of the whole approach is comparable to the one obtained with methods that are not fault-tolerant.

Interestingly, when using this algorithm, some techniques that are currently used in the field of signal processing are used for the measurement of kinematic quantities that are useful in various applications in the areas of mechanics, control, and aerospace.

Acknowledgments

The authors wish to thank Regione Piemonte (Italy) for the support provided by the CADET research program. The CADET project is coordinated by Aviospace srl, an EADS Astrium company; it is co-funded by Regione Piemonte for the programme POR FESR 2007/2013, linea di attività I.1.1. "Piattaforme innovative", AEROSPAZIO FASE II.

References

[1] E. J. Lefferts, F. L. Markley, M. D. Shuster, Kalman filtering for spacecraft attitude estimation, Journal of Guidance, Control, and Dynamics 5 (5) (1982) 417–429.

[2] P. Singla, J. L. Crassidis, J. L. Junkins, Spacecraft angular rate estimation algorithms for star tracker-based attitude determination, Advances in the Astronautical Sciences 114 (2003) 1303–1316.

[3] S. A. Hildreth, A. Arnold, Threats to us national security interests in space, in: Conference on orbital debris mitigation and removal, DTIC Document, 2014.

[4] M. D. Lichter, S. Dubowsky, State, shape, and parameter estimation of space objects from range images, in: IEEE International Conference on Robotics and Automation (ICRA), Vol. 3, IEEE, 2004, pp. 2974–2979.

[5] F. Aghili, M. Kuryllo, G. Okouneva, C. English, Fault-tolerant position/attitude estimation of free-floating space objects using a laser range sensor, Sensors Journal, IEEE 11 (1) (2011) 176–185.

[6] J. Iqbal, M. Pasha, H. K. Riaz-un Nabi, J. Iqbal, Real-time target detection and tracking: A comparative in-depth review of strategies, Life Science Journal 10 (3) (2013) 804–813.

[7] S.-M. Lim, H.-D. Kim, J.-D. Seong, Vision-based ground test for active debris removal, Journal of Astronomy and Space Sciences 30 (4) (2013) 279–290.

[8] N. Li, Y. Xu, G. Basset, N. Fitz-Coy, Tracking the trajectory of space debris in close proximity via a vision-based method, Journal of Aerospace Engineering 27 (2) (2014) 238–248.

[9] F. Terui, H. Kamimura, S. Nishida, Motion estimation to a failed satellite on orbit using stereo vision and 3d model matching, in: 9th International Conference on Control, Automation, Robotics and Vision (ICARCV), IEEE, 2006, pp. 1–8.

[10] S. Segal, A. Carmi, P. Gurfil, Stereovision-based estimation of relative dynamics between noncooperative satellites: Theory and experiments, Control Systems Technology, IEEE Transactions on 22 (2) (2014) 568–584.

[11] N. W. Oumer, G. Panin, 3d point tracking and pose estimation of a space object using stereo images, in: 21st International Conference on Pattern Recognition (ICPR), IEEE, 2012, pp. 796–800.

[12] G. Fasano, M. Grassi, D. Accardo, A stereo-vision based system for autonomous navigation of an in-orbit servicing platform, in: Infotech aerospace conference, AIAA, 2009.

[13] A. Petit, E. Marchand, K. Kanani, Tracking complex targets for space rendezvous and debris removal applications, in: IEEE/RSJ International

Conference on Intelligent Robots and Systems (IROS), IEEE, 2012, pp. 4483–4488.

[14] G. Cai, X. Chen, Z. He, Sparsity-enabled signal decomposition using tunable q-factor wavelet transform for fault feature extraction of gearbox, Mechanical Systems and Signal Processing 41 (1) (2013) 34–53.

[15] H. Tang, J. Chen, G. Dong, Sparse representation based latent components analysis for machinery weak fault detection, Mechanical Systems and Signal Processing 46 (2) (2014) 373–388.

[16] J. A. Tropp, Greed is good: Algorithmic results for sparse approximation, Information Theory, IEEE Transactions on 50 (10) (2004) 2231–2242.

[17] M. V. Afonso, J. M. Bioucas-Dias, M. A. T. Figueiredo, Fast image recovery using variable splitting and constrained optimization, Image Processing, IEEE Transactions on 19 (9) (2010) 2345–2356.

[18] C. Bonnal, M. Sanchez, W. Naumann, Ariane debris mitigation measures, in: Second European Conference on Space Debris, Vol. 393, 1997, p. 681.

[19] M. Romano, Concise form of the dynamic and kinematic solutions of the euler-poinsot problem, in: Conference on dynamics and control of space system, IAAA, 2012.

[20] B. Costic, D. Dawson, M. De Queiroz, V. Kapila, Quaternion-based adaptive attitude tracking controller without velocity measurements, Journal of Guidance, Control, and Dynamics 24 (6) (2001) 1214–1222.

[21] J. D. Foley, Introduction to computer graphics, Vol. 55.

[22] J. A. Tropp, Just relax: Convex programming methods for identifying sparse signals in noise, Information Theory, IEEE Transactions on 52 (3) (2006) 1030–1051.

[23] D. S. S. Rodrigues, M. C. Zanardi, Spacecraft attitude propagation with different representation, Advances in Space Dynamics 4 (2004) 143–150.

[24] P. L. Combettes, V. R. Wajs, Signal recovery by proximal forward-backward splitting, Multiscale Modeling & Simulation 4 (4) (2005) 1168–1200.

[25] I. Selesnick, L1-penalized least squares with salsa, Tech. rep., Connexions (2014).
URL http://cnx.org/content/m48933

[26] E. Wan, R. Van Der Merwe, et al., The unscented kalman filter for nonlinear estimation, in: Adaptive Systems for Signal Processing, Communications, and Control Symposium 2000. AS-SPCC. The IEEE 2000, IEEE, 2000, pp. 153–158.

[27] J. Hartikainen, A. Solin, S. Särkkä, Optimal filtering with kalman filters and smoothers, Department of Biomedica Engineering and Computational Sciences, Aalto University School of Science: Greater Helsinki, Finland 16.

[28] A. M. Sabatini, Kalman-filter-based orientation determination using inertial/magnetic sensors: Observability analysis and performance evaluation, Sensors 11 (10) (2011) 9182–9206.

[29] J. L. Crassidis, F. L. Markley, Unscented filtering for spacecraft attitude estimation, Journal of guidance, control, and dynamics 26 (4) (2003) 536–542.